

Probing the Structural Evolution of Gold–Aluminum Bimetallic Clusters (Au_2Al_n^- , $n = 3–11$) Using Photoelectron Spectroscopy and Theoretical Calculations

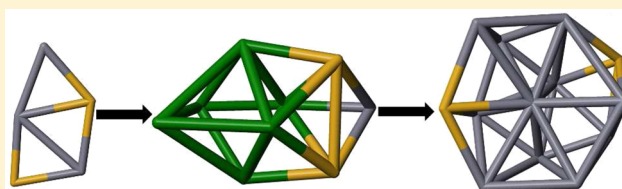
Navneet Singh Khetrpal,^{†,§} Tian Jian,^{‡,§} Gary V. Lopez,[‡] Seema Pande,[†] Lai-Sheng Wang,^{*,‡,†} and Xiao Cheng Zeng^{*,†,†}

[†]Department of Chemistry, University of Nebraska—Lincoln, Lincoln, Nebraska 68588, United States

[‡]Department of Chemistry, Brown University, Providence, Rhode Island 02912, United States

Supporting Information

ABSTRACT: We report a combined photoelectron spectroscopy and theoretical study of the structural evolution of aluminum cluster anions doped with two gold atoms, Au_2Al_n^- ($n = 3–11$). Well-resolved photoelectron spectra have been obtained at several photon energies and are used to compare with theoretical calculations to elucidate the structures of the bimetallic clusters. Global minima of the Au_2Al_n^- clusters were searched using the basin-hopping method combined with density functional theory calculations. Vertical detachment energies were computed for the low-lying isomers with the inclusion of spin–orbit effects and were used to generate simulated photoelectron spectra. Au_2Al_2^- was previously found to exhibit a *tetrahedral* structure, whereas Au_2Al_3^- is found currently to be *planar*. Beyond $n = 3$, the global minima of Au_2Al_n^- are dominated by three-dimensional structures. A robust *square-bipyramidal* Al_6 motif is observed for $n = 6–9$, leading to a highly stable tubular-like global minimum for Au_2Al_9^- . Compact three-dimensional structures are observed for $n = 10$ and 11. Except for Au_2Al_4^- , Au_2Al_6^- , and Au_2Al_7^- , the two gold atoms are separated in these digold-atom-doped aluminum clusters due to the strong Au–Al interactions.



INTRODUCTION

Size-selected clusters exhibit interesting size-dependent chemical and physical properties, and they bridge the gap between molecules and bulk materials. Owing to its high abundance and low cost, aluminum has attracted considerable research interest in cluster science. Previous studies have established that negatively charged aluminum clusters exhibit two-dimensional (2D) structures up to Al_5^- , while three-dimensional (3D) structures start to appear at Al_6^- , which is *square-bipyramidal*.¹ Al_{13}^- is known to be a magic-number cluster with *icosahedral* symmetry,^{2,3} which can resist the etching of oxygen.⁴ Metal-doping opens a new avenue to tailor the properties of metal clusters. Since the discovery of the unexpected catalytic properties of gold nanoparticles,⁵ there have also been extensive theoretical studies on the structural and electronic properties of small gold–aluminum (Au–Al) as well as other gold alloy clusters.^{6–35} It is suggested that Al atom tends to stay in the center of AlAu_n clusters, while Au atom favors peripheral sites in AuAl_n clusters. However, experimental investigations on Au–Al alloy clusters are relatively scarce. Au–Al cation clusters were first observed by mass spectrometry (MS), exhibiting electronic shell effects.^{36,37} Combined photoelectron spectroscopy (PES) and ab initio calculations revealed that AuAl_6^- featured an Au^+ capping on one triangular face of the doubly aromatic Al_6^{2-} .³⁸ In a later MS and theoretical study, AuAl_6^- was found to be chemically inert due to an electron shell closing of 20.³⁹ A joint PES and density functional theory

(DFT) study discovered that the lowest-energy isomer of AuAl_{12}^- possessed low symmetry with an interior Au atom.⁴⁰ Subsequently, another combined PES and DFT study on AuAl_{13}^- found that the Au atom caps a triangular face of Al_{13}^- .⁴¹ In a recent MS study, Au–Al cation clusters were revisited and were shown to exhibit odd–even variations in mass signals.⁴² Recently, a high-resolution PES and DFT study found that both Au_2Al_2^- and Au_2Al_2 possess C_{2v} tetrahedral structures.⁴³ Very recently, the structures of 7- and 8-membered Au_xAl_y^- clusters ($x = 1–3$; $y = 4–7$) are found to be three-dimensional (3D) via combined PES and DFT studies.⁴⁴ Again, the robust square-bipyramidal Al_6 motif was observed in AuAl_6^- , Au_2Al_6^- , and AuAl_7^- clusters. It was found that Au atoms were separated due to strong Au–Al interaction except in Au_2Al_6^- and Au_3Al_5^- .

In the current article, we report a joint PES and theoretical study on the structures of a series of aluminum cluster anions doped with two gold atoms: Au_2Al_n^- ($n = 3–11$). Note that the Au_2Al_n^- clusters with $n = 2, 5$, and 6 have been reported in previous studies,^{43,44} and they are included here for completeness. To the best of our knowledge, this is the first systematic experimental/theoretical investigation on the structural evolution of double-gold-atom-doped aluminum clusters.

Received: May 23, 2017

Revised: July 25, 2017

Published: July 26, 2017

EXPERIMENTAL METHODS

The experiment was performed using a magnetic-bottle PES apparatus equipped with a laser vaporization source, details of which have been published elsewhere.^{45,46} Briefly, the gold–aluminum anions were produced by laser vaporization of an Au/Al composite target. Clusters formed in the nozzle were entrained in the helium carrier gas seeded with 5% argon gas and underwent a supersonic expansion to produce cold clusters.⁴⁷ After passing through a skimmer, anion clusters were extracted from the cold collimated molecular beam into a time-of-flight mass spectrometer. Clusters of interest were mass-selected, decelerated, and photodetached by the 193 nm (6.424 eV) radiation from an ArF excimer laser, and the 266 nm (4.661 eV) and the 355 nm (3.496 eV) radiation from a Nd:YAG laser. Photoelectrons were collected at nearly 100% efficiency by a magnetic bottle and analyzed in a 3.5 m long electron flight tube. Photoelectron spectra were calibrated by using the known spectra of Au⁻ or Bi⁻. The energy resolution of the apparatus was $\Delta E_k/E_k \approx 2.5\%$, that is, approximately 25 meV for 1 eV electrons.

THEORETICAL METHODS

The basin-hopping (BH) global optimization method⁴⁸ in conjugation with DFT calculations was used to search global minima of the Au₂Al_{*n*}⁻ (*n* = 3–11) clusters. During the BH search, structures of local minima following each accepted move were optimized using the Perdew–Burke–Ernzerhof exchange correlation functional⁵¹ with the Gaussian double- ζ plus polarization function (DNP) basis set implemented in the DMol3 4.0 program.^{49,50} The top 35 low-energy isomers obtained from the BH global optimization were considered as candidates for the lowest-lying structures. These candidates were further reoptimized using the PBE0 functional⁵² with the aug-cc-pVDZ basis set⁵³ implemented in the Gaussian09 package.⁵⁴ Apart from the lowest multiplicity, three higher multiplicities were also considered at this step. The high-multiplicity structures were used in the next step only if their relative energies are within 0.2 eV of the lowest-energy structures. During the reoptimization for each cluster, some of the structures were found to converge to the same geometry, resulting in a total number of candidates less than 35. Harmonic vibrational frequencies were calculated at the same level of theory in order to ensure that the obtained structures are true minima.

Next, single-point energy computations of the reoptimized geometries were performed using the PBE0 functional with aug-cc-pVDZ basis set implemented in the NWChem 6.6 package⁵⁶ with inclusion of the spin–orbit (SO) effects for the gold atoms. The inclusion of SO effects for gold has been proven to give a quantitative match between the experimental and simulated PES spectra for gold–aluminum alloy as well as pure gold anion clusters.^{44,55} The first vertical detachment energy (VDE) was calculated as the energy difference between the neutral and anion at the PBE0-optimized anion geometry. The binding energies of deeper occupied orbitals were added to the first VDE to generate electronic density of states. Each VDE was fitted with a Gaussian of 0.035 eV width to yield simulated PES spectra, which were compared with the experimental PES spectra to identify the lowest-energy structures. The energy gap (eV) between the first and second highest occupied molecular orbitals (HOMO1 and HOMO2), representing the gap between peaks labeled X and A, was also calculated for all the candidate isomers. In addition, single-point energy calculations at the

CCSD(T)^{57,58} (coupled-cluster method including singles, doubles, and noniterative perturbative triple) level with the aug-cc-pVDZ basis set, implemented in the G09 package, were performed to determine the best candidate isomers in cases where more than one candidate isomer was identified to closely match the experimental spectrum. Hereafter, the PBE0/aug-cc-pVDZ, PBE0/aug-cc-pVDZ//SO-PBE0/aug-cc-pVDZ, and PBE0/aug-cc-pVDZ//CCSD(T)/aug-cc-pVDZ levels of theory are referred to as PBE0, SO-PBE0, and CCSD(T), respectively.

RESULTS AND DISCUSSION

The photoelectron spectra of Au₂Al_{*n*}⁻ (*n* = 3, 4, 7–11) at three photon energies are shown in Figure 1. The spectra for *n* = 5 and 6 have been reported recently in a study of 7- and 8-membered Au_{*x*}Al_{*y*}⁻ clusters (*x* = 1–3; *y* = 4–7).⁴⁴ The observed features are labeled by letters X, A, B, C, ... in Figure 1, where X denotes the transition from the ground state of the anion to that of the neutral and A, B, C, ... denote detachment transitions to the excited states of the neutral cluster. Weak features labeled with prime and * indicate contributions from minor isomers and impurities, respectively. The experimental VDEs are measured from the maximum of each band and are summarized in Tables S1–S7 as Supporting Information.

Figure 2 shows the change of experimental first VDEs and theoretical first VDEs of the assigned isomers with respect to number of aluminum atoms. The theoretical VDEs show excellent agreement with the experimental values with the average deviation of 0.070 eV. This shows that the selected level of theory is appropriate for the Au₂Al_{*n*}⁻ species in the current study.

Au₂Al₃⁻. The 355 nm spectrum of Au₂Al₃⁻ (Figure 1a) shows two bands X and A. Band X is quite sharp with a VDE of 2.03 eV, while band A is slightly broader at a VDE of 3.06 eV. The energy gap between X and A is 1.03 eV. The 266 nm spectrum (Figure 1b) reveals two more bands “*” and B, at VDEs of 2.75 and 3.61 eV, respectively. The weak band * exhibits strong photon-energy dependence, being slightly more intense at 266 nm. This weak photon-energy-dependent signal was likely derived from either two-electron processes⁵⁹ or impurity. After band B, the signal-to-noise ratio is poor, so no more features can be assigned in Figure 1b. In 193 nm spectrum (Figure 1c), almost continuous signals were observed beyond 4 eV and a band C is tentatively labeled around 5.1 eV. All measured VDEs are given in Table S1.

Figure 3a displays the 193 nm photoelectron spectrum of Au₂Al₃⁻, compared with the simulated spectra of the top-three candidate isomers. The singlet isomer II possesses a 2D structure, while triplet isomer I and singlet isomer VIII exhibit 3D structures. As shown in Tables 1 and S8, at the PBE0 level, the triplet isomer I is the most stable, while at the SO-PBE0 level, isomers I–IV are close in energy with isomer III lying the lowest. At the CCSD(T) level, isomers I, II, and VIII are competing for the most stable structure with isomer II being the lowest lying. Despite a systematic red shift by 0.242 eV, isomer II can well reproduce all the main features in the experimental spectrum. This red shift in the computed VDE with respect to the experiment is consistent with our previous study on Au₂Al₅⁻,⁴⁴ which might also be resulting from the inclusion of spin–orbit coupling in the SO-PBE0 calculation. While the calculated first VDE is close to the experimental value, isomer III (simulated spectrum shown in Figure S1 and relative energy data in Table S8) is too high in the CCSD(T) relative energy and also misses feature B in the simulated

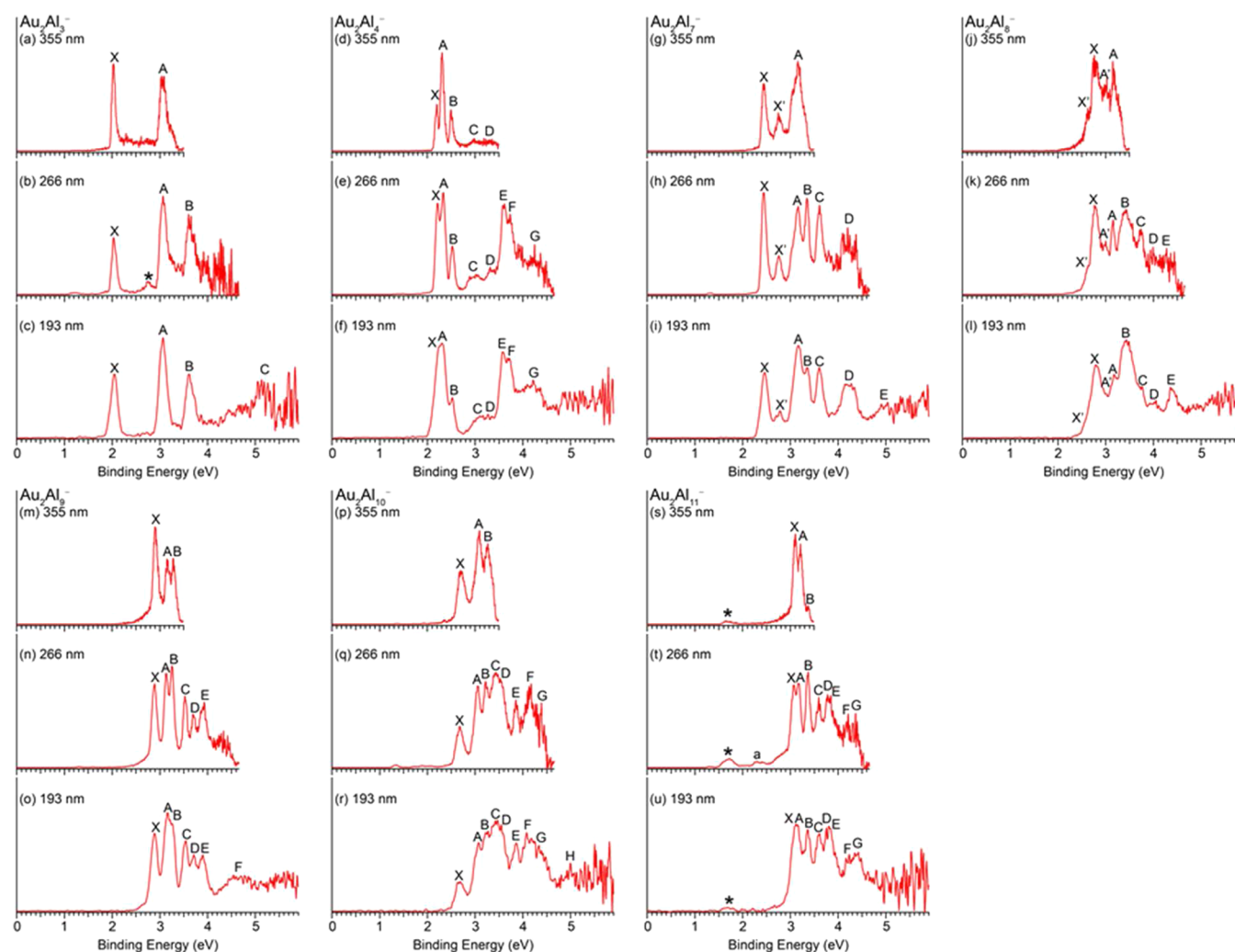


Figure 1. Experimental photoelectron spectra of Au_2Al_n^- ($n = 3, 4, 7-11$) at three photon energies.

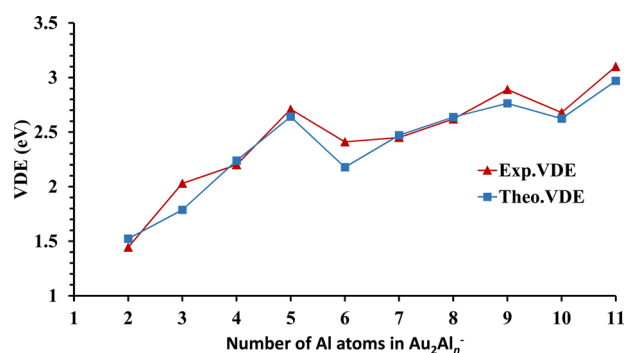


Figure 2. Experimental and theoretical VDEs of Au_2Al_n^- ($n = 2-11$) versus the number of aluminum atoms.

spectrum. Isomers I and VIII can be excluded due to the overestimated X–A gap and the missing of band B (or unreasonably large A–B gap in comparison to experiment). Hence, we conclude that the planar singlet isomer II is the most stable structure for Au_2Al_3^- .

Au_2Al_4^- . The 355 nm spectrum (Figure 1d) shows three sharp and closely spaced bands X, A, and B at VDEs of 2.20, 2.32, and 2.52 eV, respectively. Followed by a small energy gap after band B, two broad and weak bands C and D are observed around 3.0 and 3.3 eV. The 266 nm spectrum (Figure 1e)

reveals three more bands E, F, and G. Bands E and F are intense and sharp, lying close to each other at 3.60 and 3.73 eV. The broad band G is observed to be at ~ 4.3 eV. The 193 nm spectrum (Figure 1f) shows no more well-resolved bands, except nearly continuous signals with relatively poor signal-to-noise ratios. The weak features C and D are likely due to a minor isomer or two-electron processes. All measured VDEs are given in Table S2.

Figure 3b displays the 193 nm photoelectron spectrum of Au_2Al_4^- , compared with the simulated spectra of the top three candidate isomers. Isomer I is the global minimum at both DFT and CCSD(T) levels (Table 1); its simulated spectrum can reproduce the major features of X, A, B, E, F, and G in the experimental spectrum. The weak features C and D are absent in the simulated spectrum of isomer I, and they are probably from a minor isomer. Isomer IV can be a good candidate for the minor isomer as its simulated spectrum can reproduce not only bands C and D but also the continuous signals around 5 eV which seem to be absent in the case of isomer II. The global minimum of Au_2Al_4^- consists of an Al-capped pentagonal structure, reminiscent of the previously reported bicapped pentagonal structure for Au_2Al_5^- .⁴⁴ Overall, isomers I and IV can be assigned as the major and minor species observed experimentally, respectively.

Au₂Al₇⁻. The 355 nm spectrum (Figure 1g) shows three well-resolved bands, labeled as X, X', and A. Bands X (VDE: 2.45 eV) and A (VDE: 3.16 eV) are quite intense. The band X' at a VDE of 2.76 eV is relatively weak, suggesting that it may result from a minor isomer. There seems to be an unresolved shoulder in the low binding energy side of band A. The 266 nm spectrum (Figure 1h) reveals two more well-resolved bands B and C with VDEs of 3.35 and 3.61 eV, respectively. Following a small energy gap from C, a broad band D at 4.2 eV is observed. The 193 nm spectrum (Figure 1i) displays continuous signals beyond 5.0 eV. Band E is tentatively labeled for the sake of discussion. All measured VDEs are given in Table S3.

Figure 3c displays the 193 nm photoelectron spectrum of Au₂Al₇⁻, compared with the simulated spectra of the top two candidate isomers. Among the candidate isomers obtained from the BH search, isomers I–VI are all close in energies at the PBE0 level, while isomer II is the lowest in energy at the SO-PBE0 and CCSD(T) levels (Table 1). The simulated spectrum of isomer II can also reproduce all the main features (X, A–E) observed experimentally. Isomers I, III, and IV (simulated spectra shown in Figure S3) can be excluded as the major contributor because their calculated first VDEs are all too high. Isomer I is 0.215 eV higher than isomer II at the CCSD(T) level, and it seems to account for band X' and the unresolved shoulder of band A. Thus, isomer II can be assigned as the major isomer, while isomer I can be assigned as the minor isomer for Au₂Al₇⁻. It should be pointed out that the Al₆ square bipyramid motif is preserved in all the low-lying isomers of Au₂Al₇⁻. The structure of isomer II is similar to the reported major isomer of Au₂Al₆⁻ with one more Al atom bonded to the two gold atoms.

Au₂Al₈⁻. The 355 nm spectrum (Figure 1j) is quite congested, displaying two intense bands (X and A) and two weak bands (X' and A'). The VDEs of bands X and A are measured to be 2.78 and 3.16 eV, respectively. Band X' is on the shoulder of band X with a VDE of 2.62 eV. Band A' is located between bands X and A, with a VDE of 3.00 eV. The relatively weak intensities of bands X' and A' suggest they may come from minor isomers. The 266 nm spectrum (Figure 1k) reveals four more bands B, C, D, and E. Band B at 3.42 eV is

quite broad, which may contain several detachment transitions. The sharper band C is well-resolved at a VDE of 3.74 eV, while bands D and E exhibit poor signal-to-noise ratios in 266 nm spectrum. At 193 nm (Figure 1l), bands D and E are better defined, with VDEs at 4.05 and 4.37 eV, respectively. Beyond band E, the PES signals are almost continuous, and no definitive PES bands can be identified. All measured VDEs are given in Table S4.

Figure 3d displays the 193 nm photoelectron spectrum of Au₂Al₈⁻, compared with the simulated spectra of the top three candidate isomers. The relative energy differences among isomers I–IV are very small at the PBE0 level, with isomer I being the lowest (Table S11). At the SO-PBE0 level, isomers II, IV, and VI are almost degenerate in energy with isomer II being the lowest-lying isomer. At the CCSD(T) level, isomers III and IV are competing for the global minimum, while isomer I lies slightly higher by 0.144 eV and isomer II becomes much higher in energy and can be excluded.

The photoelectron spectra of Au₂Al₈⁻ are very complicated with strong evidence of the presence of multiple isomers. On the basis of the simulated spectrum, isomer III can be tentatively assigned as the major isomer because it can well reproduce the main bands X, A–C, and E. Isomer V can be assigned as a minor isomer as its simulated spectrum can account for bands X' and A'. Being almost degenerate with isomer III at the CCSD(T) level, isomer IV cannot be ruled out and it may also contribute to band A'. Thus, three isomers may be populated in the cluster beam of Au₂Al₈⁻. It is interesting to note that the square-bipyramidal Al₆ motif is also present in isomers III and V.

Au₂Al₉⁻. The 193 nm spectrum (Figure 1m) shows three well-resolved bands X, A, and B, with VDEs of 2.89, 3.15, and 3.28 eV, respectively. The 266 nm spectrum (Figure 1n) displays three more bands C, D, and E at VDEs of 3.53, 3.70, and 3.92 eV, respectively. The 193 nm spectrum (Figure 1r) reveals essentially continuous signals beyond 4 eV. A broad band F at ~4.7 eV is tentatively labeled. The spectra of Au₂Al₉⁻ are relatively well resolved with sharp PES bands, suggesting a relatively stable structure with little or no isomer present in the cluster beam. All measured VDEs are given in Table S5.

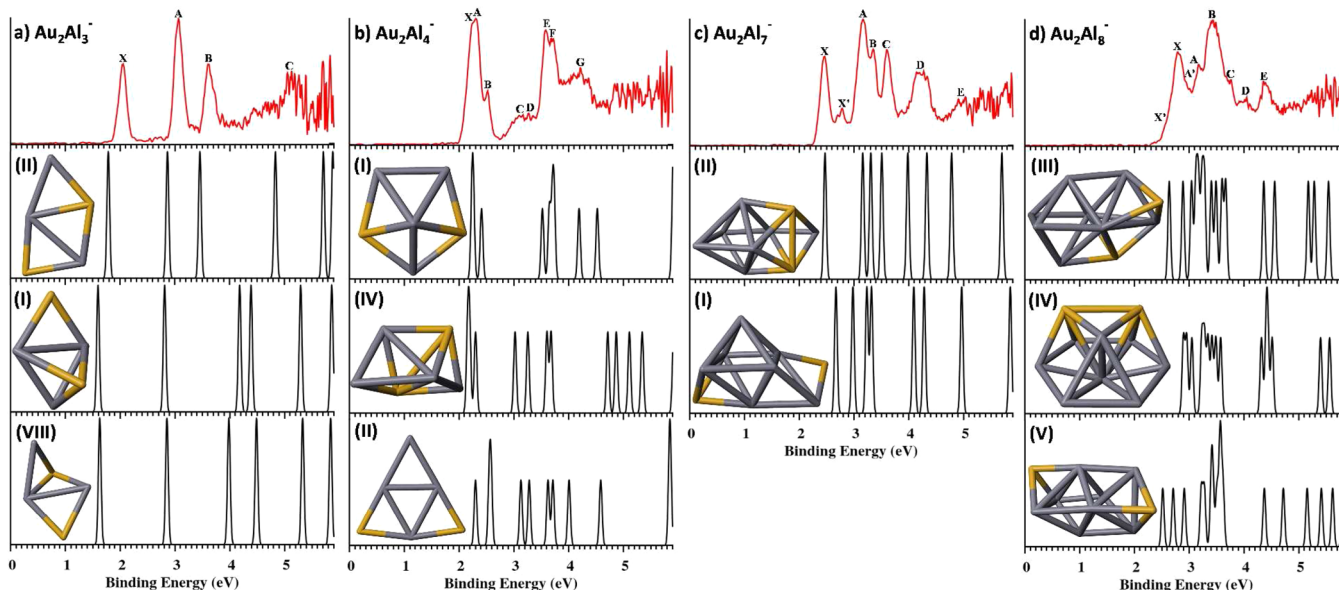


Figure 3. Comparison of the simulated spectra with the 193 nm experimental spectra for the low-lying isomers of Au₂Al_n⁻ ($n = 3, 4, 7$, and 8). The aluminum and gold atoms are in gray and gold color, respectively.

Table 1. Experimental First VDE (eV) (the X Band in Figure 1), the Energy Gap (eV) between the Peaks X and A from the 193 nm Experimental Spectra for Au_2Al_n^- ($n = 3, 4, 7-11$), Isomers Studied, Their Point Groups and Relative Energies (eV) Computed at the PBE0/aug-cc-pVDZ, SO-PBE0/aug-cc-pVDZ, CCSD(T)/aug-cc-pVDZ Levels (with All Isomers Being Optimized at the PBE0/aug-cc-pVDZ Level), Theoretical First VDE (eV), and the Energy Gap (eV) between HOMO1 and HOMO2 Orbitals (Corresponding to the Gap between Peaks X and A)

anion cluster	experimental				theoretical					
	VDE ^a	gap	isomer	point group	ΔE (PBE0/aug-cc-pVDZ)	ΔE (SO-PBE0/aug-cc-pVDZ)	ΔE (CCSD(T)/cc-pVDZ)	VDE	gap	
Au_2Al_3^-	2.03(4)	1.03	II	C_s	0.154	0.021	0.000	1.788	1.081	
			I	C_s	0.000	0.097	0.055	1.595	1.217	
			VIII	C_1	0.219	0.103	0.084	1.626	1.228	
Au_2Al_4^-	2.20(4)	0.12	I	C_s	0.000	0.000	0.000	2.239	0.024	
			II	C_{2v}	0.179	0.158	0.303	2.302	0.254	
			IV	C_1	0.316	0.273	0.313	2.16	0.035	
Au_2Al_7^-	2.45(3)	0.71	II	C_s	0.011	0.000	0.000	2.472	0.69	
			I	C_1	0.000	0.169	0.215	2.671	0.311	
Au_2Al_8^-	2.78(2)	0.38	III	C_1	0.060	0.118	0.000	2.638	0.252	
			IV	C_s	0.093	0.067	0.012	2.897	0.06	
			V	C_2	0.108	0.237	0.198	2.518	0.191	
Au_2Al_9^-	2.89(2)	0.26	VI	C_1	0.019	0.000	0.000	2.764	0.267	
			I	C_1	0.000	0.192	0.339	2.897	0.151	
$\text{Au}_2\text{Al}_{10}^-$	2.68(2)	0.39	I	C_1	0.000	0.000	0.000	2.625	0.320	
			II	C_1	0.006	0.123	0.000	2.731	0.223	
$\text{Au}_2\text{Al}_{11}^-$	3.10(1)	0.11	I	C_1	0.000	0.007	0.008	2.97	0.064	
			V	C_1	0.061	0.009	0.000	2.851	0.294	
			VIII	C_s	0.095	0.050	0.009	2.744	0.311	

^aNumbers in parentheses represent the uncertainty in the last digit.

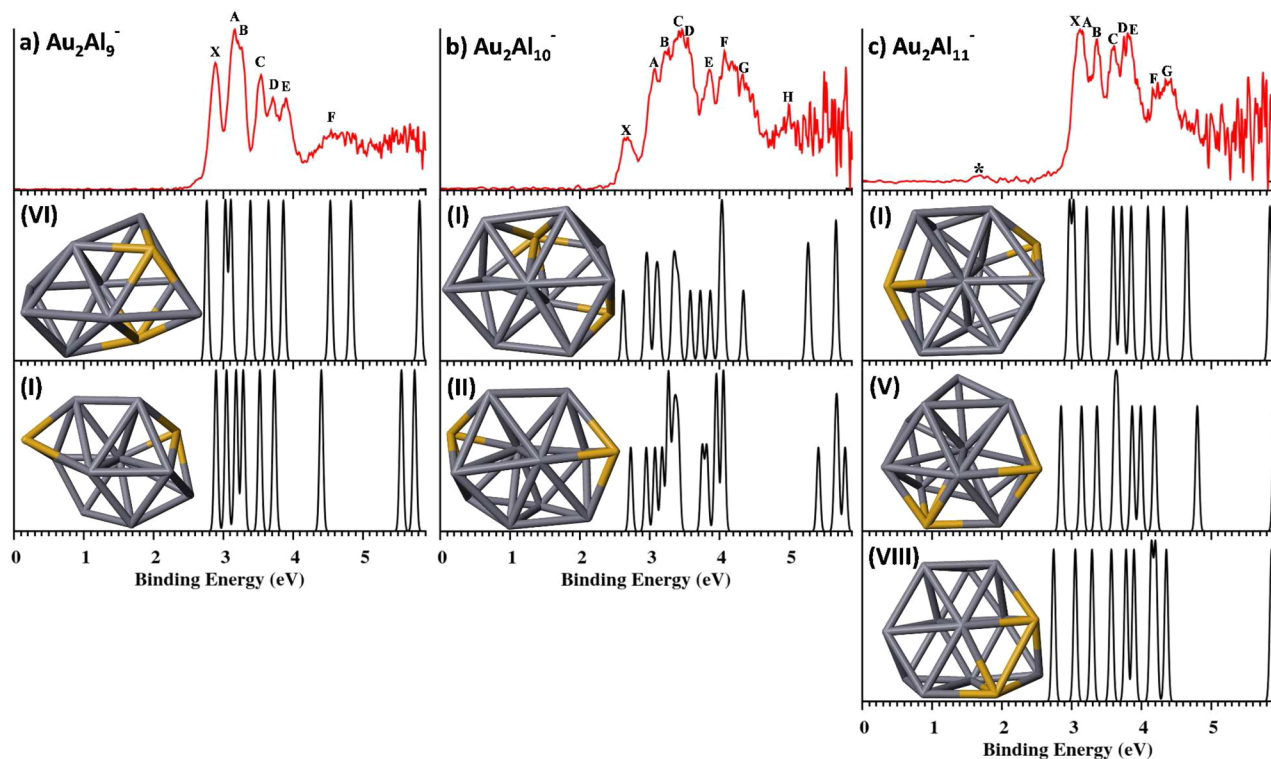


Figure 4. Comparison of the simulated spectra with the 193 nm experimental spectra for the low-lying isomers of Au_2Al_n^- ($n = 9-11$). The aluminum and gold atoms are in gray and gold color, respectively.

Figure 4a displays the 193 nm photoelectron spectrum of Au_2Al_9^- , compared with the simulated spectrum of the top two candidate isomers. Among the examined candidate isomers, isomers I–VI are very close in energy at the PBE0 level (Table S12). However, isomer VI becomes appreciably more

stable at both the SO-PBE0 and CCSD(T) levels (Table 1). At the CCSD(T) level, all other isomers are at least 0.17 eV higher in energy, suggesting the exceptional stability of isomer VI. The simulated spectrum of isomer VI is almost in quantitative agreement with the experimental spectrum, firmly confirming

isomer VI as the global minimum of Au_2Al_9^- . On the basis of both the energetics (Table S12) and the simulated spectra (Figures S6 and S7), all other isomers can be ruled out. Despite the tubular shape of isomer VI, a square-bipyramidal Al_6 motif can still be recognized.

$\text{Au}_2\text{Al}_{10}^-$. The 355 nm spectrum (Figure 1p) displays three well-resolved bands. The ground state band X is observed at a VDE of 2.68 eV. Following a small energy gap from band X, two closely spaced bands A and B are observed at VDEs of 3.07 and 3.22 eV, respectively. The 266 nm spectrum (Figure 1q) reveals many more PES bands, showing a rather congested spectrum. Bands C and D at VDEs 3.45 and 3.54 eV overlap with each other and are not well resolved. Bands E and F have VDEs at 3.85 and 4.13 eV, respectively. Band G at ~ 4.3 eV is not well resolved in the 266 nm spectrum, but only slightly better defined in 193 nm spectrum (Figure 1r), which basically reveals continuous signals beyond 4.6 eV. Band H at ~ 5.0 eV is tentatively labeled. All measured VDEs are given in Table S6.

Figure 4b displays the 193 nm photoelectron spectrum of $\text{Au}_2\text{Al}_{10}^-$, compared with the simulated spectrum of the top two candidate isomers. The potential energy landscape of $\text{Au}_2\text{Al}_{10}^-$ is much more complicated. Isomers I–III and VIII are almost degenerate at both DFT and CCSD(T) levels (Table S13), making it rather difficult to compare with the experiment.

The simulated spectra for other isomers are given in Figure S8, and only the simulated spectra of the two nearly degenerate isomers I and II are compared with the experiment in Figure 4b. Isomer I can account for the major observed PES bands, while isomer II cannot be ruled out. The experimental spectra are relatively well resolved, suggesting that it is unlikely that other isomers are populated appreciably in the cluster beam. Thus, isomer I is tentatively assigned as global minimum for $\text{Au}_2\text{Al}_{10}^-$, which possesses a compact 3D structure.

$\text{Au}_2\text{Al}_{11}^-$. The 355 nm spectrum (Figure 1s) exhibits two intense and closely spaced bands (X and A) at VDEs of 3.10 and 3.21 eV, respectively. The feature “*” at 1.68 eV might result from an impurity or a photodissociation product of the parent anion. A weak band B is observed near the threshold, which is better resolved at 266 nm (Figure 1x), which reveals five more congested bands. A weak band “a” observed at 2.30 eV corresponds to detachment of Au^- , indicating the possibility of photodissociation. No new PES bands are observed in the 193 nm spectrum (Figure 1x), which shows continuous signals beyond band G. All measured VDEs are given in Table S7.

Figure 4c displays the 193 nm photoelectron spectrum of $\text{Au}_2\text{Al}_{11}^-$, compared with the simulated spectra of the top three candidate isomers. The potential landscape of $\text{Au}_2\text{Al}_{11}^-$ is also very complicated. The relative energies of isomers I–VIII are

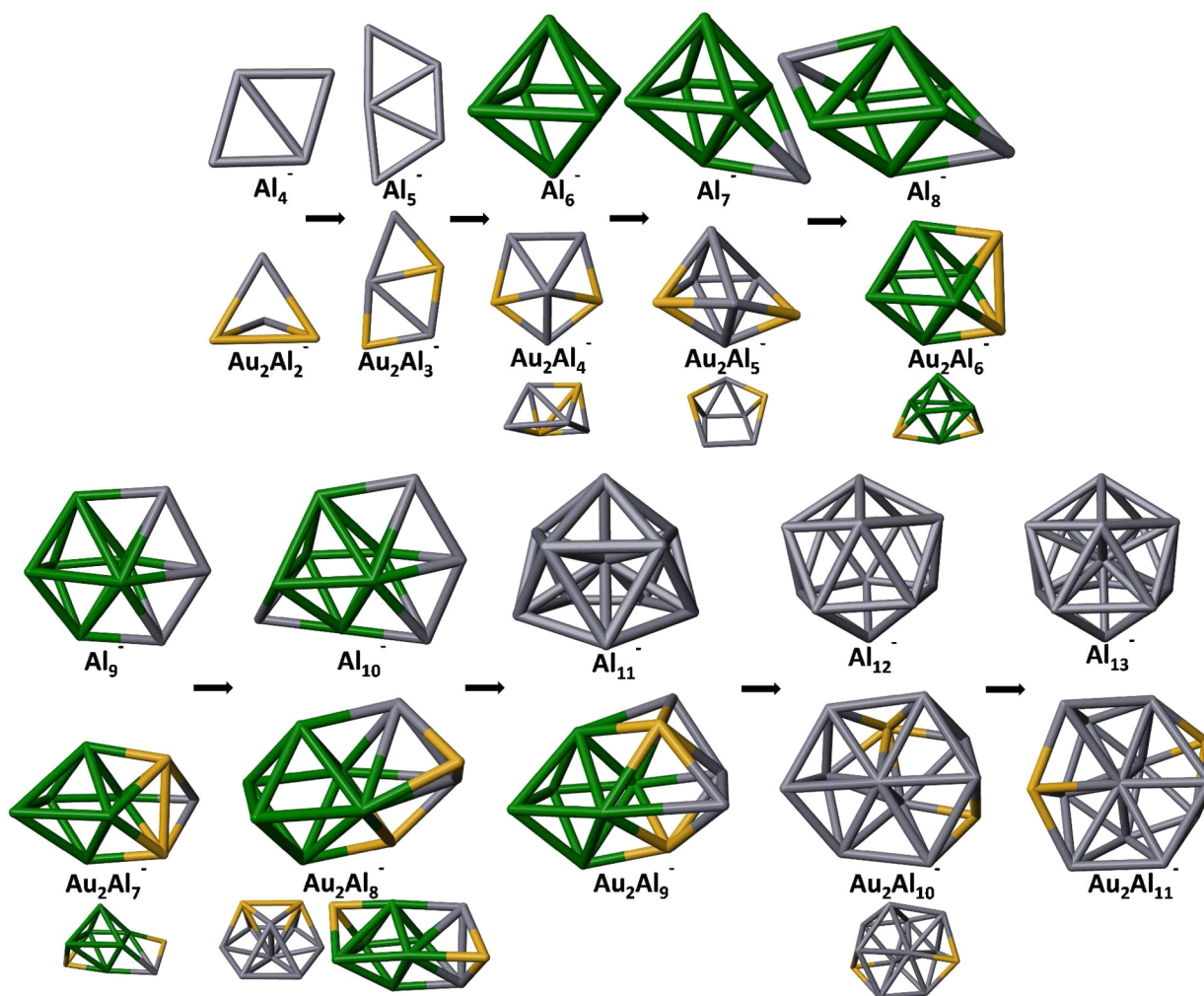


Figure 5. Structural evolution of pure aluminum Al_{n+2}^- and di-Au-doped Al clusters Au_2Al_n^- ($n = 2-11$). The size of the minor isomers has been kept smaller than that of the major isomers. Atom color code: Au (gold color) and Al (gray or green color). The Al atoms in green color highlight the highly stable square-bipyramidal Al_6^- motif.

very close at both the DFT and CCSD(T) levels (Table S14). The simulated spectra of isomers I, V, and VIII, which are lowest in energy at CCSD(T), are compared with the experiment in Figure 4c, while those for other isomers are given in Figures S9 and S10. The simulated spectrum of isomer I is in good agreement with the observed spectrum, suggesting that it constitutes the major isomer in the experiment. While isomers V and VIII cannot be ruled out, no distinct PES bands can be attributed to them, suggesting that their populations in the cluster beam would be small if present. Isomer I of $\text{Au}_2\text{Al}_{11}^-$ also has a compact 3D structure similar to $\text{Au}_2\text{Al}_{10}^-$.

Structural Evolution of Au_2Al_n^- ($n = 2-11$). The identified global minimum structures for the digold-doped aluminum cluster anions and the corresponding pure aluminum cluster anions (Al_{n+2}^-) are shown in Figure 5. The structures of Au_2Al_n^- ($n = 2, 5$ and 6) and Al_{n+2}^- ($n = 2-11$) are from the previous studies.^{43,44,60} There are a number of interesting structural features in this size range. The structures of the bimetallic clusters evolve from 3D at $n = 2$ to 2D at $n = 3$ and then 3D beyond $n = 3$. The Au_2Al_3^- is found to have an interesting 2D structure, which optimizes Au–Al interactions and is reminiscent of the 2D structure of Al_5^- .¹ The 3D structures reappear at Au_2Al_4^- for both its global minimum and its minor isomer. In the recent study,⁴⁴ we found that the highly symmetric square-bipyramidal Al_6 motif³⁸ is present in AuAl_6^- , Au_2Al_6^- , and AuAl_7^- . In the current study, we find that this Al_6 motif persists in the global minima from Au_2Al_7^- to Au_2Al_9^- . In the case of pure aluminum cluster anions, the Al_6 motif is found in the Al_6^- to Al_{10}^- size range. The global minimum of Au_2Al_7^- can be viewed as being formed from the major isomer of Au_2Al_6^- with the additional Al atom added to the side of the two gold atoms. The global minimum of Au_2Al_8^- contains a square-bipyramidal Al_6 unit with two adjacent triangular faces capped by Al and Au atom and an Al–Au–Al unit, respectively. The global minimum of Au_2Al_9^- has a tubular shape, containing a distorted square-bipyramidal Al_6 motif at one end. This tubular structure is found to be particularly stable. The structures of $\text{Au}_2\text{Al}_{10}^-$ and $\text{Au}_2\text{Al}_{11}^-$ exhibit compact 3D features, which are similar to the single Au-doped AuAl_{12}^- cluster.⁴⁰ The two Au atoms of $\text{Au}_2\text{Al}_{10}^-$ and $\text{Au}_2\text{Al}_{11}^-$ occupy peripheral sites, while that of AuAl_{12}^- was found to be in the interior position.⁴⁰ The structures of Au_2Al_9^- , $\text{Au}_2\text{Al}_{10}^-$, and $\text{Au}_2\text{Al}_{11}^-$ are quite different from their pure aluminum cluster counterparts (Al_{11}^- , Al_{12}^- , and Al_{13}^-). In order to compare the Au–Au, Al–Al, and Au–Al interactions, we plot the average Mayer bond orders (MBO) for the Au–Au, Al–Al, and Au–Al bonds versus the number of aluminum atoms in Figure 6. For a given Au_2Al_n^- cluster, the average MBO value of the Au–Al bonds is larger than that of

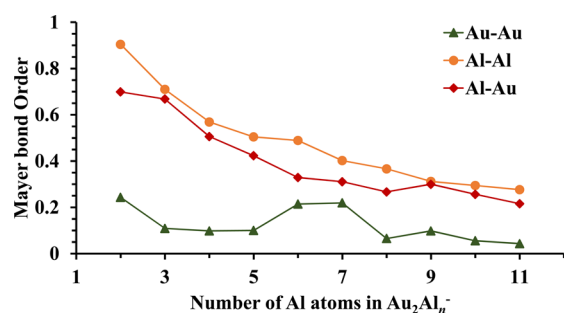


Figure 6. Average Mayer bond orders for the Au–Au, Al–Al, and Au–Al bonds versus the size of the di-Au-doped Al cluster anions Au_2Al_n^- ($n = 2-11$).

Au–Au bonds but smaller than that of the Al–Al bonds, suggesting that the Au–Al interactions are more dominant than the Au–Au interactions so that there is no direct Au–Au bonding in the Au_2Al_n^- ($n = 2-11$) clusters. The Au_2Al_6^- and Au_2Al_7^- clusters are exceptions, where the robustness of the Al_6 motif dominates the energetic requirement for Au–Au separation in the bimetallic Au–Al clusters.

Relative Stabilities and Charge Distribution. To explore the relative structural stabilities of the double-gold-doped aluminum cluster anions Au_2Al_n^- ($n = 2-11$), we plot the average binding energies (E_b) and the second-order energy difference (Δ^2E) versus the cluster size (number of aluminum atoms) in Figure 7. CCSD(T) energies of the most stable isomers

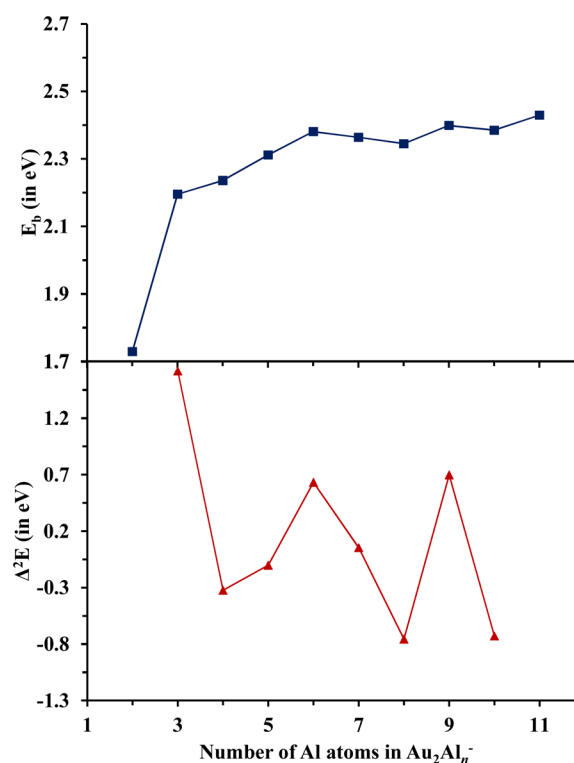


Figure 7. Size dependence of average binding energies (E_b) and second-order energy differences (Δ^2E) for the most stable di-Au-doped Al cluster anions Au_2Al_n^- ($n = 2-11$).

(singly assigned or major isomers) were used for these calculations. The E_b and Δ^2E of Au_2Al_n^- clusters are defined as follows

$$E_b = [E(\text{Au}) + E(\text{Au}^-) + nE(\text{Al})]/(n + 2)$$

$$\Delta^2E = E(\text{Au}_2\text{Al}_{n-1}^-) + E(\text{Au}_2\text{Al}_{n+1}^-) - 2E(\text{Au}_2\text{Al}_n^-)$$

where E is the energy of corresponding atom, ion, or cluster. The average binding energy per atom shows a sharp increase from $n = 2$ to $n = 3$ and a gradual increase afterward with addition of more aluminum atoms, suggesting that the cluster formation is more favorable for bigger values of n . The variation of the second-order energy difference with the cluster size shows local peaks at Au_2Al_6^- and Au_2Al_9^- , indicating that these clusters appear to be more stable than their neighboring-sized clusters.

In order to analyze the charge distribution, we performed the natural population analysis for the most stable isomers of the Au_2Al_n^- ($n = 2-11$) at the PBE0/aug-cc-pvdz level of theory. The variation of charge on gold atoms with respect to the number aluminum atoms is presented in Figure 8. For each

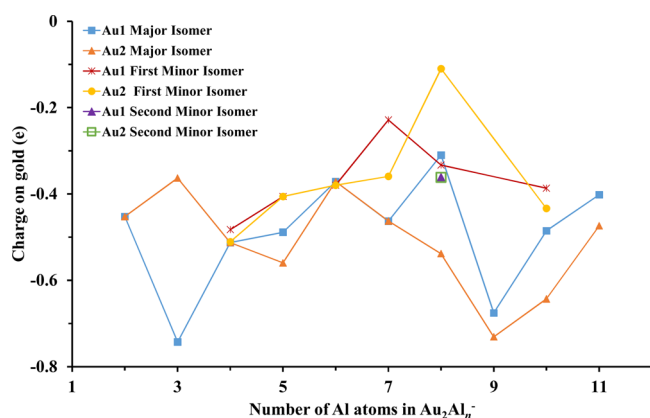


Figure 8. Negative charge on gold atoms versus the size of the di-Au-doped Al cluster anions Au_2Al_n^- ($n = 2-11$).

cluster size, higher negative charge resides on the two gold atoms. This is expected as gold has a higher electronegativity than the aluminum.

CONCLUSION

In conclusion, we present a joint experimental and theoretical study on double-gold-atom-doped aluminum cluster anions Au_2Al_n^- ($n = 3, 4, 7-11$). Well-resolved photoelectron spectra were obtained for these clusters and used to compare with theoretical calculations for structure elucidation. The potential-energy landscapes of these bimetallic clusters are found to be quite complicated, and multiple isomers are observed and identified in a number of clusters. The *square-bipyramidal* Al_6 motif is found to be a dominating structural feature for $n = 6-9$. The Au_2Al_9^- is found to be a highly stable tubular type structure. The $\text{Au}_2\text{Al}_{10}^-$ and $\text{Au}_2\text{Al}_{11}^-$ clusters are found to exhibit compact three-dimensional structures. Except for Au_2Al_4^- , Au_2Al_6^- , and Au_2Al_7^- , the two gold atoms are separated in these double-gold-atom-doped aluminum clusters due to the strong Au–Al interactions. Relative stabilities of the identified most stable bimetallic clusters are analyzed via computing their binding energy and the second-order energy difference as a function of cluster size. By comparing the charge distribution with cluster structures, we find that the gold atom coordinated with higher number of aluminum atoms tends to possess higher electron density.

ASSOCIATED CONTENT

Supporting Information

The Supporting Information is available free of charge on the ACS Publications website at DOI: 10.1021/acs.jpcc.7b04997.

Tables S1–S14 and Figures S1–S10 as described in the text; XYZ coordinates of the assigned isomers (PDF)

AUTHOR INFORMATION

Corresponding Authors

*E-mail: Lai-Sheng_Wang@brown.edu.

*E-mail: xzeng1@unl.edu.

ORCID

Lai-Sheng Wang: 0000-0003-1816-5738

Xiao Cheng Zeng: 0000-0003-4672-8585

Author Contributions

[§]These authors contributed equally to this work.

Notes

The authors declare no competing financial interest.

ACKNOWLEDGMENTS

The experiment done at Brown University was supported by the National Science Foundation (CHE-1263745 to L.S.W.). X.C.Z. was supported by a grant from Nebraska Center for Energy Sciences Research. The calculations were done in the Holland Computing Center at University of Nebraska—Lincoln. T. J. thanks Dr. Wei-Li Li for earlier experimental assistance.

REFERENCES

- Rao, B.; Jena, P. Evolution of the Electronic Structure and Properties of Neutral and Charged Aluminum Clusters: A Comprehensive Analysis. *J. Chem. Phys.* **1999**, *111*, 1890–1904.
- Li, X.; Wu, H.; Wang, X. B.; Wang, L. S. S-P Hybridization and Electron Shell Structures in Aluminum Clusters: A Photoelectron Spectroscopy Study. *Phys. Rev. Lett.* **1998**, *81*, 1909.
- Akola, J.; Manninen, M.; Häkkinen, H.; Landman, U.; Li, X.; Wang, L. S. Photoelectron Spectra of Aluminum Cluster Anions: Temperature Effects and Ab Initio Simulations. *Phys. Rev. B: Condens. Matter Mater. Phys.* **1999**, *60*, R11297.
- Leuchtner, R.; Harms, A.; Castleman, A., Jr Thermal Metal Cluster Anion Reactions: Behavior of Aluminum Clusters with Oxygen. *J. Chem. Phys.* **1989**, *91*, 2753–2754.
- Haruta, M. Size- and Support-Dependency in the Catalysis of Gold. *Catal. Today* **1997**, *36* (1), 153–166.
- Pyykkö, P.; Zhao, Y. Relativistic Pseudopotential Calculation of Bonding Trends in XAu_n^{m+} Clusters ($X = \text{B-N, Al-S}$; $n = 4-6$). *Chem. Phys. Lett.* **1991**, *177*, 103–106.
- Urban, B. M.; Sadlej, J. A. Binding of Aluminium to Coinage Metals: Electron Correlation and Relativistic Effects. *Mol. Phys.* **1997**, *92*, 587–600.
- Zope, R. R.; Baruah, T. Conformers of Al_{13} , Al_{12}M , and Al_{13}M ($\text{M} = \text{Cu, Ag, and Au}$) Clusters and Their Energetics. *Phys. Rev. A: At, Mol., Opt. Phys.* **2001**, *64*, 053202.
- Majumder, C.; Kandalam, A. K.; Jena, P. Structure and Bonding of Au_5M ($\text{M} = \text{Na, Mg, Al, Si, P, and S}$) Clusters. *Phys. Rev. B: Condens. Matter Mater. Phys.* **2006**, *74*, 205437.
- Chen, M. X.; Yan, X.; Wei, S. Al_7Ag and Al_7Au Clusters with Large Highest Occupied Molecular Orbital–Lowest Unoccupied Molecular Orbital Gap. *J. Phys. Chem. A* **2007**, *111*, 8659–8662.
- Liu, F.; Zhao, Y.; Li, X.; Hao, F. Ab Initio Study of Structure and Stability of M_2Al_2 ($\text{M} = \text{Cu, Ag, and Au}$) Clusters. *Aust. J. Chem.* **2007**, *60*, 184–189.
- Zhao, L. X.; Feng, X. J.; Cao, T. T.; Liang, X.; Luo, Y. H. Density Functional Study of Al-Doped Au Clusters. *Chin. Phys. B* **2009**, *18*, 2709.
- Rajesh, C.; Majumder, C. Oxidation of Al Doped Au Clusters: A First Principles Study. *J. Chem. Phys.* **2009**, *130*, 234309.
- Zhao, L. X.; Cao, T. T.; Feng, X. J.; Lei, Y. M.; Luo, Y. H.; Xiao-Liang, A. Theoretical Study of Neutral and Anionic Au_3Al Clusters. *J. Mol. Struct.: THEOCHEM* **2009**, *895*, 92–95.
- Zhang, M.; Chen, S.; Deng, Q.; He, L.; Zhao, L.; Luo, Y. Structures and Electronic Properties of M@Au_6 ($\text{M} = \text{Al, Si, P, S, Cl, Ar}$) Clusters: A Density Functional Theory Investigation. *Eur. Phys. J. D* **2010**, *58*, 117–123.
- Li, Y. F.; Mao, A. J.; Li, Y.; Kuang, X. Y. Density Functional Study on Size-dependent Structures, Stabilities, Electronic and Magnetic Properties of Au_nM ($\text{M} = \text{Al and Si}$, $n = 1-9$) Clusters: Comparison with Pure Gold Clusters. *J. Mol. Model.* **2012**, *18*, 3061–3072.
- Wang, C. J.; Kuang, X. Y.; Wang, H. Q.; Li, H. F.; Gu, J. B.; Liu, J. Density-Functional Investigation of the Geometries, Stabilities, Electronic, and Magnetic Properties of Gold Cluster Anions Doped with Aluminum: Au_nAl^- ($1 \leq n \leq 8$). *Comput. Theor. Chem.* **2012**, *1002*, 31–36.
- Yao, W. Z.; Liu, B. T.; Lu, Z. H.; Li, S. D. Bridging Gold in Electron-Deficient $\text{Al}_2\text{Au}_n^{-/0}$ and $\text{BAu}_n^{-/0}$ ($n = 1-3$) Clusters. *J. Phys. Chem. A* **2013**, *117*, 5178–5183.

- (19) Guo, L.; Li, S. Y.; Zhang, X.; Zhang, R. J.; Guo, J. Hydrogen Adsorption and Dissociation on Small Al_nAu Clusters: An Electronic Structure Density Functional Study. *Eur. Phys. J. D* **2013**, *67*, 1–11.
- (20) Li, Y. F.; Li, Y.; Kuang, X. Y. Probing the Structural and Electronic Properties of Bimetallic Group-III Metal-Doped Gold Clusters: Au_nM_2 ($M = Na, Mg, Al; n = 1-8$). *Eur. Phys. J. D* **2013**, *67*, 132.
- (21) Zhang, M.; Yang, S. B.; Feng, X. J.; Zhao, L. X.; Zhang, H. Y.; Luo, Y. H. Structural Stability and Electronic Properties of Small Gold Clusters Induced by 3p Electron Atoms. *Eur. Phys. J. D* **2013**, *67*, 11.
- (22) Guo, L.; Yang, Y.; Wen, C.; Dong, X.; Ren, N.; Niu, S. First-principle Calculations on CO Oxidation Catalyzed by Subnanometer $AlAu_n$ Clusters. *Mater. Chem. Phys.* **2014**, *147*, 504–513.
- (23) Li, S.; Guo, L.; Zhang, R.; Zhang, X. Structures, Stabilities, and Electronic Properties of Al_nAu ($n = 1-15$) Clusters: A Density Functional Study. *J. Struct. Chem.* **2014**, *55*, 612–620.
- (24) Yao, W. Z.; Lu, Z. H.; Li, S. D. A Comparative Ab Initio Study of the Geometric and Electronic Structures of B_2Au_4 , Al_2Au_4 and $BAlAu_4$. *Acta Phys.-Chim. Sin.* **2014**, *30*, 2233–2240.
- (25) An, X.; Guo, L.; Li, A. A DFT Study of the CO Oxidation Mechanism on Al_nAu ($n = 1-12$) Clusters. *J. Cluster Sci.* **2015**, *26*, 505–527.
- (26) Bhattacharjee, D.; Mishra, B. K.; Deka, R. C. Effect of Double Aluminium Doping on the Structure, Stability, and Electronic Properties of Small Gold Clusters. *J. Mater. Sci.* **2015**, *50*, 4586–4599.
- (27) Li, A.; Guo, L.; An, X.; Liu, N.; Cao, Z.; Li, W.; Zheng, X.; Shi, Y.; Guo, J.; Xi, Y. The Catalytic Mechanism of CO Oxidation in $AlAu$ Clusters Determined by Density Functional Theory. *J. Struct. Chem.* **2016**, *57*, 54–64.
- (28) Wang, X.; Adeleke, A. A.; Cao, W.; Luo, Y.; Zhang, M.; Yao, Y. Structures of Nanoalloy Clusters Au_nAl_m ($n = 1-10$) and the Growth Patterns to the Bulk Phase. *J. Phys. Chem. C* **2016**, *120*, 25588–25595.
- (29) Wang, L. M.; Pal, R.; Huang, W.; Zeng, X. C.; Wang, L. S. Tuning the Electronic Properties of the Golden Buckyball by Endohedral Doping: $M@ Au_{16}^-$ ($M = Ag, Zn, In$). *J. Chem. Phys.* **2009**, *130*, 051101.
- (30) Pal, R.; Wang, L. M.; Huang, W.; Wang, L. S.; Zeng, X. C. Structural Evolution of Doped Gold Clusters: MAu_x^- ($M = Si, Ge, Sn; x = 5-8$). *J. Am. Chem. Soc.* **2009**, *131*, 3396–3404.
- (31) Wang, L. M.; Bai, J.; Lechtken, A.; Huang, W.; Schooss, D.; Kappes, M. M.; Zeng, X. C.; Wang, L. S. Magnetic Doping of the Golden Cage Cluster $M@ Au_{16}^-$ ($M = Fe, Co, Ni$). *Phys. Rev. B: Condens. Matter Mater. Phys.* **2009**, *79*, 033413.
- (32) Wang, L. M.; Bulusu, S.; Huang, W.; Pal, R.; Wang, L. S.; Zeng, X. C. Doping the Golden Cage Au_{16}^- with Si, Ge, and Sn. *J. Am. Chem. Soc.* **2007**, *129*, 15136–15137.
- (33) Wang, L. M.; Bulusu, S.; Zhai, H. J.; Zeng, X. C.; Wang, L. S. Doping Golden Buckyballs: $Cu@ Au_{16}^-$ and $Cu@ Au_{17}^-$ Cluster Anions. *Angew. Chem., Int. Ed.* **2007**, *46*, 2915–2918.
- (34) Gao, Y.; Bulusu, S.; Zeng, X. C. A Global Search of Highly Stable Gold-Covered Bimetallic Clusters $M@ Au_n$ ($n = 8-17$): Endohedral Gold Clusters. *ChemPhysChem* **2006**, *7*, 2275–2278.
- (35) Wang, L. M.; Pal, R.; Huang, W.; Zeng, X. C.; Wang, L. S. Observation of Earlier Two-to-Three Dimensional Structural Transition in Gold Cluster Anions by Isoelectronic Substitution: MAu_n^- ($n = 8-11; M = Ag, Cu$). *J. Chem. Phys.* **2010**, *132*, 114306.
- (36) Bouwen, W.; Vanhoutte, F.; Despa, F.; Bouckaert, S.; Neukermans, S.; Kuhn, L. T.; Weidele, H.; Lievens, P.; Silverans, R. E. Stability Effects of $Au_nX_m^+$ ($X = Cu, Al, Y, In$) Clusters. *Chem. Phys. Lett.* **1999**, *314*, 227–233.
- (37) Heinebrodt, M.; Malinowski, N.; Tast, F.; Branz, W.; Billas, L.; Martin, T. Bonding Character of Bimetallic Clusters Au_nX_m ($X = Al, In, Cs$). *J. Chem. Phys.* **1999**, *110*, 9915–9921.
- (38) Kuznetsov, A. E.; Boldyrev, A. I.; Zhai, H. J.; Li, X.; Wang, L. S. Al_6^{2-} —Fusion of Two Aromatic Al_3 -Units. A Combined Photoelectron Spectroscopy and Ab Initio Study of $M^+[Al_6^{2-}]$ ($M = Li, Na, K, Cu, and Au$). *J. Am. Chem. Soc.* **2002**, *124*, 11791–11801.
- (39) Kimble, M. L.; Castleman, A. W.; Reveles, J. U.; Khanna, S. N. On the Magic Character of Al_6Au . *Collect. Czech. Chem. Commun.* **2007**, *72*, 185–196.
- (40) Pal, R.; Cui, L. F.; Bulusu, S.; Zhai, H. J.; Wang, L. S.; Zeng, X. C. Probing the Electronic and Structural Properties of Doped Aluminum Clusters: MAu_{12}^- ($M = Li, Cu, and Au$). *J. Chem. Phys.* **2008**, *128*, 024305.
- (41) Ko, Y. J.; Shakya, A.; Wang, H.; Grubisic, A.; Zheng, W.; Götz, M.; Ganteför, G.; Bowen, K. H.; Jena, P.; Kiran, B. Electronic Structure and Properties of Isoelectronic Magic Clusters: Al_3X ($X = H, Au, Li, Na, K, Rb, Cs$). *J. Chem. Phys.* **2010**, *133*, 124308.
- (42) King, B.; Moore, J.; Veryovkin, I.; Pellin, M. High Sensitivity Sputter Neutral Mass Spectrometry—Sputtering of Neutral Mixed Clusters from Gold–aluminum Alloys. *Nucl. Instrum. Methods Phys. Res., Sect. B* **2013**, *317*, 115–120.
- (43) Lopez, G. V.; Czekner, J.; Jian, T.; Li, W. L.; Yang, Z.; Wang, L. S. Probing the Electronic and Vibrational Structure of $Au_2Al_2^-$ and Au_2Al_2 using Photoelectron Spectroscopy and High Resolution Photoelectron Imaging. *J. Chem. Phys.* **2014**, *141*, 224309.
- (44) Khetrapal, N. S.; Jian, T.; Pal, R.; Lopez, G. V.; Pande, S.; Wang, L. S.; Zeng, X. C. Probing the Structures of Gold–Aluminum Alloy Clusters $Au_nAl_m^-$: A Joint Experimental and Theoretical Study. *Nanoscale* **2016**, *8*, 9805–9814.
- (45) Wang, L. S.; Cheng, H. S.; Fan, J. Photoelectron Spectroscopy of Size-Selected Transition Metal Clusters: Fe_n^- , $n = 3-24$. *J. Chem. Phys.* **1995**, *102*, 9480–9493.
- (46) Wang, L. S. Photoelectron Spectroscopy of Size-Selected Boron Clusters: From Planar Structures to Borophenes and Borospherenes. *Int. Rev. Phys. Chem.* **2016**, *35*, 69–142.
- (47) Huang, W.; Wang, L. S. Probing the 2D to 3D Structural Transition in Gold Cluster Anions Using Argon Tagging. *Phys. Rev. Lett.* **2009**, *102*, 153401.
- (48) Wales, D. J.; Doye, J. P. K. Global Optimization by Basin-Hopping and the Lowest Energy Structures of Lennard-Jones Clusters Containing up to 110 Atoms. *J. Phys. Chem. A* **1997**, *101* (28), 5111–5116.
- (49) Delley, B. An All-electron Numerical Method for Solving the Local Density Functional for Polyatomic Molecules. *J. Chem. Phys.* **1990**, *92*, 508–517.
- (50) Delley, B. From Molecules to Solids with the DMol3 Approach. *J. Chem. Phys.* **2000**, *113*, 7756–7764.
- (51) Perdew, J. P.; Burke, K.; Ernzerhof, M. Generalized Gradient Approximation Made Simple. *Phys. Rev. Lett.* **1996**, *77*, 3865–3868.
- (52) Ernzerhof, M.; Scuseria, G. E. Assessment of the Perdew–Burke–Ernzerhof Exchange–Correlation Functional. *J. Chem. Phys.* **1999**, *110*, 5029–5036.
- (53) Dunning, T. H. Gaussian Basis Sets for Use in Correlated Molecular Calculations. I. The Atoms Boron through Neon and Hydrogen. *J. Chem. Phys.* **1989**, *90*, 1007–1023.
- (54) Frisch, M. J.; Trucks, G. W.; Schlegel, H. B.; Scuseria, G. E.; Robb, M. A.; Cheeseman, J. R.; Scalmani, G.; Barone, V.; Mennucci, B.; Petersson, G. A.; et al. *Gaussian 09*; Gaussian, Inc.: Wallingford, CT, 2009.
- (55) Shao, N.; Huang, W.; Gao, Y.; Li, X.; Wang, L. S.; Zeng, X. C.; Wang, L. M. Probing the Structural Evolution of Medium-Sized Gold Clusters: Au_n^- ($n = 27-35$). *J. Am. Chem. Soc.* **2010**, *132*, 6596–6605.
- (56) Valiev, M.; Bylaska, E. J.; Govind, N.; Kowalski, K.; Straatsma, T. P.; Van Dam, H. J. J.; Wang, D.; Nieplocha, J.; Apra, E.; Windus, T. L.; et al. A NWChem: A comprehensive and Scalable Open-Source Solution for Large Scale Molecular Simulations. *Comput. Phys. Commun.* **2010**, *181*, 1477–1489.
- (57) Purvis, G. D., III; Bartlett, R. J. A Full Coupled-Cluster Singles and Doubles Model: The Inclusion of Disconnected Triples. *J. Chem. Phys.* **1982**, *76*, 1910–1918.
- (58) Scuseria, G. E.; Janssen, C. L.; Schaefer, H. F., III An Efficient Reformulation of the Closed-Shell Coupled Cluster Single and Double Excitation (CCSD) Equations. *J. Chem. Phys.* **1988**, *89*, 7382–7387.

(59) Süzer, S.; Lee, S. T.; Shirley, D. A. Correlation Satellites in the Atomic Photoelectron Spectra of Group-IIA and -IIB Elements. *Phys. Rev. A: At, Mol, Opt. Phys.* **1976**, *13*, 1842–1849.

(60) Xing, X.; Wang, J.; Kuang, X.; Xia, X.; Lu, C.; Maroulis, G. Probing the Low-Energy Structures of Aluminum-Magnesium Alloy Clusters: A Detailed Study. *Phys. Chem. Chem. Phys.* **2016**, *18*, 26177–26183.